Phase Behavior of Poly(9,9-di-*n*-hexyl-2,7-fluorene)

S. H. Chen

Department of Materials Science and Engineering, National Dong Hwa University, Hualien 974, Taiwan

A. C. Su* and C. H. Su

Institute of Materials Science and Engineering and Center for Nanoscience and Nanotechnology, National Sun Yat-sen University, Kaohsiung 804, Taiwan

S. A. Chen

Department of Chemical Engineering, National Tsing Hua University, Hsinchu 300, Taiwan

Received: September 28, 2005; In Final Form: January 15, 2006

Here we report the phase behavior of poly(9,9-di-*n*-hexyl-2,7-fluorene) (PFH), which previously received little attention as compared to its homologues poly(9,9-di-*n*-octyl-2,7-fluorene) (PFO) and poly(9,9-di-(2′-ethylhexyl)-2,7-fluorene) (PFEH). By means of differential scanning calorimetry, X-ray diffraction, and electron microscopy, we show that there exist four different phases in PFH. The as-cast film is mainly composed of a mesomorphic β phase with layer spacing of ca. 1.4 nm. This β phase is inherently metastable and, upon heating above 175 °C, transforms into a crystalline (α) form that melts into a nematic (N) liquid above 250 °C. Upon stepwise cooling, the nematic melt crystallizes into the α phase first, followed by solid−solid transformation into another crystalline (α') form. Unit cell structure of the α form is monoclinic whereas that of the α' form is triclinic, but departures from strict orthogonality are slight (by ca. 6°). These observations not only support our previous assignment of two crystalline forms (both orthorhombic in structure) in PFO but also provide insights to the crystalline nature of the polyfluorene series.

Introduction

Due to their potential applications in electroluminescent displays, polyfluorenes (PFs, general chemical structure inset in Figure 7b, in which a variety of alkyl substitutions R_1 and R_2 can be attached to the bridgehead carbon) have attracted much attention.[1−3] Within the PF family, poly(9,9-di-*n*-octyl-2,7-fluorene) (PFO, with $R_1 = R_2 =$ *n*-octyl) is most extensively studied and shown to be semicrystalline with a melting temperature (T_m) around 160 °C, above which a nematic (N) mesophase exists up to an isotropization temperature T_i = ca. 300 °C.[4−7] There may also be a mesomorphic β phase in the as-cast film or upon solvent vapor treatment of the nematic phase.[8,9] Since these phases can be selectively maintained via proper selection of processing parameters,[4,8,9] the resulting "morphological effects" in light-emission properties have been extensively examined.[10−19] On the basis of transmission electron microscopic (TEM) and X-ray diffraction (XRD) results,[20] we recently proposed a structural model for the crystalline (α) phase of PFO as orthorhombic ($a = 2.56$ nm, $b = 2.34$ nm, $c = 3.32$ nm, space group $P2_12_12_1$) with 8 chains (each of four fluorene repeats) in the unit cell. We have further suggested[21] the presence of a modified crystalline (α') form, which is also orthorhombic in structure but kinetically favored at melt−crystallization temperatures (T_c) lower than 130 °C and lower in T_m as compared to the α form. The modification involves the lowered symmetry (i.e., increased order) in molecular packing and a slight increase in the *b*-dimension to 2.38 nm, in addition to the interesting habit of preferential orientation of the *a*-axis along the film normal. Nevertheless, in view of the similarities between the α and the α' phases of PFO, one might wonder if the distinction between the two phases is significant. Here we show that the polymorphic nature of PFO extends in fact to a close homologue, poly(9,9-di-*n*-hexyl-2,7-fluorene) (PFH, with $R_1 = R_2 =$ *n*-hexyl), for which the two crystalline polymorphs are more distinctively different in structure and hence unambiguously identifiable. In addition, the transformation between the two crystalline forms is shown to occur reversibly upon thermal cycling. These observations not only support our previous assignment of two crystalline forms in PFO but also provide insights to the crystalline nature of the polyfluorene series.

Experimental Section

The PFH sample used here was purchased from American Dye Source, Quebec, Canada. The weight-average molecular mass (M_w) was 45 kDa (with polydispersity index PDI = 2.8) as determined from size exclusion chromatography with polystyrene standards; a more realistic estimate could be $M_w = 17$ kDa if the correction factor (2.7^{-1}) from small-angle light scattering results of Grell et al.[8] for PFO is used.

Differential scanning calorimetric (DSC) measurements were made by use of a TA Q100 instrument routinely calibrated with indium and lead standards and operated under a stream of nitrogen gas. For the X-ray diffraction (XRD) study, a Bruker D8 Advance diffractometer equipped with a copper target (Kα-line, with wavelength $\lambda = 0.154$ nm), a graphite collimator, and a vacuumed high-temperature stage (Anton Paar TTK-450) was used under a step-scan rate of 0.05° per 3 s in the scattering angle range of $2\theta = 2°$ to 41°. Full range calibration of scattering angles was made with use of silicon and silver

10.1021/jp0555145 CCC: $33.50
Published on Web 02/08/2006

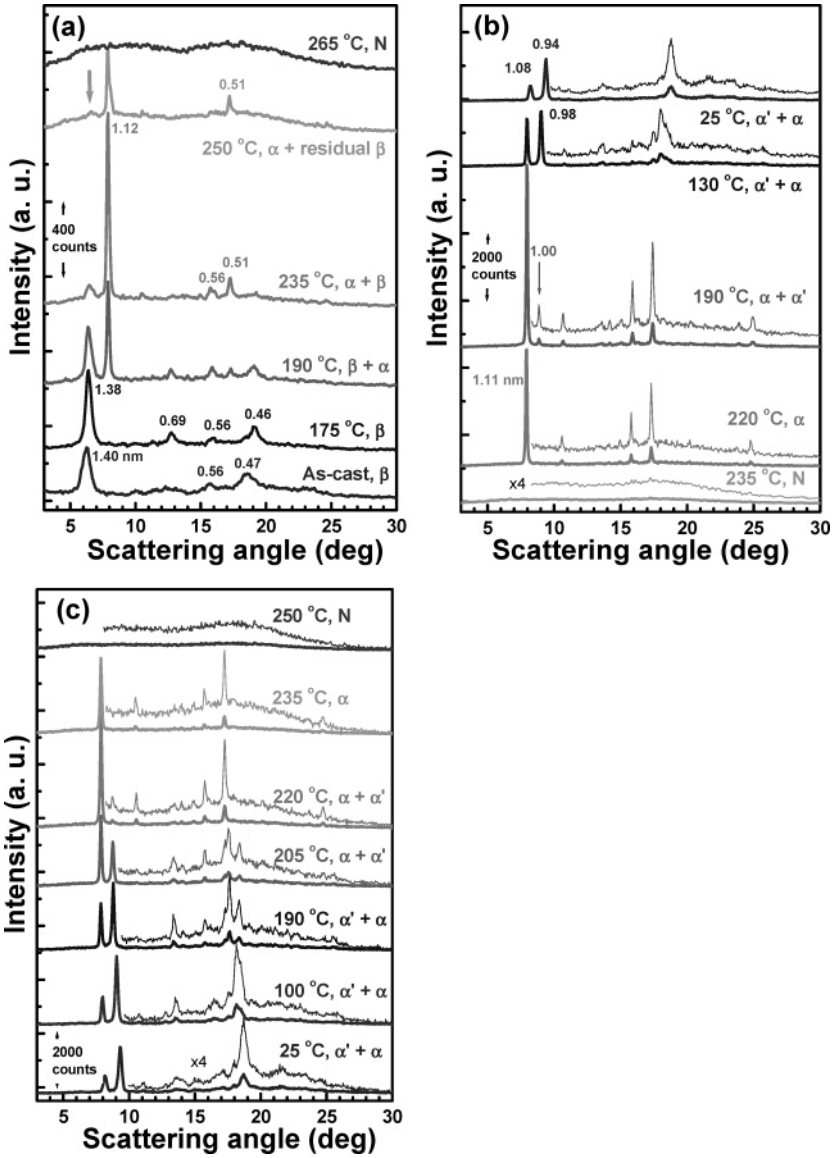

Figure 1. Representative XRD profiles obtained (a) for cast PFH film (from 1% toluene solution a day after its preparation) upon stepwise increases in temperature (at intervals of 15 °C) from ambient to 265 °C, initially showing improvement but then disappearance of smectic-like (β) order with emergence of the crystalline (α) phase that melts into nematic liquid above ca. 250 °C, and (b) during subsequent cooling (also at 15 °C intervals) to room temperature, showing α-to-α' transformation. (c) XRD profiles in the second round of stepwise heating (at intervals of 15 °C) from ambient to 265 °C. Note that the given intensity scales are intended for thick lines; thinner lines in panels b and c are expanded four times in intensity for clarity.

behenate standards. Transmission electron microscopic (TEM) studies were performed with a JEOL 3010 instrument under an acceleration voltage of 200 kV. Due to beam damages, the lifetime of electron diffraction patterns under high magnifications is generally short (on the order of 5 s). This calls for focusing at one point of the specimen and exposure at a nearby point upon a slight shift of specimen position. Surface topographic features of the TEM specimens were examined via secondary electron images (SEI) obtained by use of a field emission scanning electron microscope (FESEM, JEOL JSM-6330TF) under an accelerating voltage of 10 kV.

Films were drop-cast from dilute (generally ca. 0.1 w/v % for TEM specimens and 1 w/v % for XRD studies) solutions of PFH in toluene on glass or quartz substrates. These were subjected to a short stay at 280 °C to erase previous processing history; this is followed by (1) jumping to an isothermal crystallization temperature for a period of time and subsequent quenching in ice water or (2) programmed cooling at 20 °C/min to room temperature. After heat treatment in the Linkman high-temperature stage, specimens (ca. 50 nm in thickness) for TEM studies were floated off the glass substrate with a dilute HF solution and subsequently vacuum coated/shadowed with C/Pt.

Results and Discussion

Phase Identifications. The XRD profile of the as-cast film generally shows features of a lamellar mesomorph (coined as the β phase following the nomenclature adopted for PFO) ca. 1.4 nm in layer spacing (bottom curve in Figure 1a and top curve in Figure 2a). With increasing storage time of the solution before casting, there may exist additional weak reflections (such as the one ca. 0.56 nm in d spacing, Figure 1a) that are not attributable to higher order reflections in the lamellar harmonics. For films cast from freshly prepared solutions, these extraneous peaks become less discernible (Figure 2a). These observations imply that, within the mesomorphic β matrix, there may be a minor presence of solvent induced but poorly developed

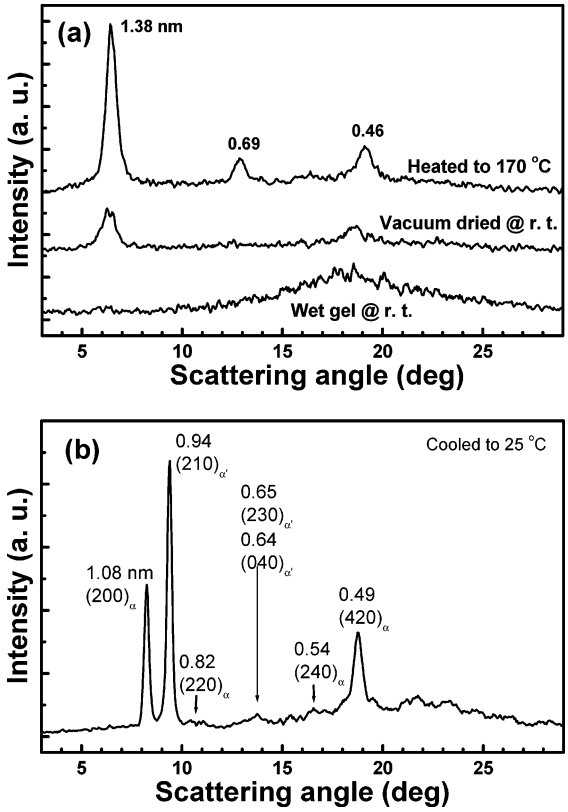

Figure 2. (a) XRD profiles during film formation and upon heating to 170 °C, showing the mesomorphic order (β phase) in the as-cast film and the subsequent improvement in lamellar packing. The film was cast from a freshly prepared hot (ca. 85 °C) solution of 1% PFH in toluene. (b) Expanded view of the XRD profile (top curve in Figure 1b) after stepwise cooling to room temperature from the nematic state. Characteristic reflections are indexed according to respective pseudo-orthorhombic unit cells of α and α′ phases, as constructed from SAED analysis.

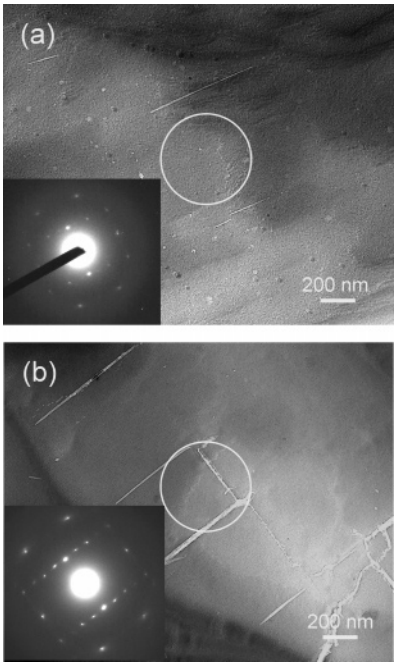

Figure 3. BFI and corresponding SAED [00*l*] zonal patterns (as insets) of PFH specimens crystallized at 230 °C for 15 h, followed by (a) quenching in ice−water or (b) programmed cooling at 20 °C/min to room temperature. Circles near the center denote locations where the SAED pattern was taken, which correspond to the aperture size of 0.5 μm. Note the differences in the SAED patterns, which signify the sole presence of the α phase (a) and the coexistence of α and α′ phases (b). White stripes (enhanced by Pt-shadowing) running parallel to the *a*- and the *b*-axes in panel b correspond to tensile and compressive cracks, respectively, that are attributable to stresses induced by the α-to-α′ transformation. Expanded and indexed views of the SAED patterns are more clearly given in Figures 5a and 6a.

crystalline (presumably clathrate) domains as previously proposed for PFO[22] or in a more remote case[23] of poly(2-methoxy-5-(2′-ethylhexyloxy)-1,4-phenylenevinylene) (MEH-PPV). Upon increases in temperature up to 175 °C, the lamellar order is significantly improved (second curve from the bottom of Figure 1a and middle curve in Figure 2a) without discernible improvement in the solvent-induced crystalline order, consistent with the assignment of two different phases.

As the temperature is raised beyond 175 °C (subsequent curves in Figure 1a), the β phase transforms into crystalline order, as indicated by the decrease in intensity of the characteristic lamellar reflections and the simultaneous emergence of a multiple of sharp reflections, particularly the one ca. 1.1 nm in *d* spacing. We coin this crystalline phase the α form, which becomes better developed at 235 °C, starts to dissipate at 250 °C, and finally melts into the nematic phase (as confirmed by independent observations via polarized light microscopy) above 260 °C. Note that there remains some residual β mesophase even at 250 °C. In the subsequent cooling steps (cf. Figure 1b), the recrystallized α phase appears first at 220 °C; the process progresses upon cooling to 190 °C but then there emerges an additional phase (coined the α′ phase) characterized by the new reflection ca. 1.0 nm in *d* spacing. This new reflection intensifies at the expense of the α phase upon further decreases in temperature. In the second-round heating of the same specimen up to 250 °C (again at intervals of 15 °C, Figure 1c), one observes transformation of the α′ phase to the α phase at temperatures between 190 and 220 °C; the latter phase subsequently melts at ca. 250 °C into the nematic order. The XRD profiles in the cooling sequence to follow are essentially the same as those given in Figure 1b (and hence not shown), demonstrating reversibility of transformation between the two crystalline polymorphs. Note that the β phase is *intrinsically metastable*: once dissipated upon heating, it never reappears in the absence of solvents.

The assignment of two crystalline forms is supported by TEM evidence given in Figures 3−6. Representative bright field images (BFI) and the corresponding selected-area electron diffraction (SAED) patterns for specimens quenched in liquid nitrogen (α phase, Figure 3a) or program-cooled at 20 °C/min (coexistence of α and α′ phases, Figure 3b) after being isothermally crystallized at 230 °C are shown in Figure 3. Corresponding BFI and "fiberlike" SAED patterns for shear-oriented specimens are shown in Figure 4. For the α phase, the expanded views (Figure 5) of the SAED patterns indicate clear features of monoclinic unit cell structure with $a = 2.15$ nm, $b = 2.47$ nm, $c = 3.32$ nm, and $\alpha = 96°$. Note that reflection conditions of $h + k =$ even values in Figure 5a indicate the presence of a 2-fold screw symmetry along the *a*-axis or a *b*-glide plane perpendicular to the *a*-axis whereas off-axis reflections in the "fiber" pattern of the shear oriented specimen (Figure 5b) are largely extinct, implying ordering mainly in the two-dimensional (2D) positioning of the backbones and translational symmetry (disorder) along the backbones. In other words, PFH chains in the α phase bear some mesomorphic nature and may be comfortably displaced along the backbone without disrupting the 2D positional order in the *a*−*b* plane, reminiscent of conformationally disordered ("condis") crystals

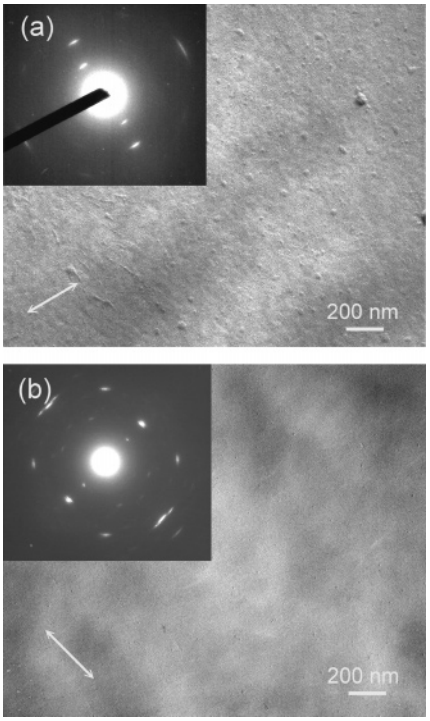

Figure 4. BFI and corresponding SAED patterns of PFH specimens manually sheared at 280 °C, followed by melt crystallization (a) at 225 °C for 1 h before quenching in ice−water (for controlled formation of the α form) or (b) at 170 °C for 10 min before programmed cooling to room temperature (for coexistence of α and α′ forms). Double-headed arrows indicate the direction of shear. Specimens were lightly shadowed with Pt. Expanded and indexed views of the SAED patterns are more clearly given in Figures 5b and 6b.

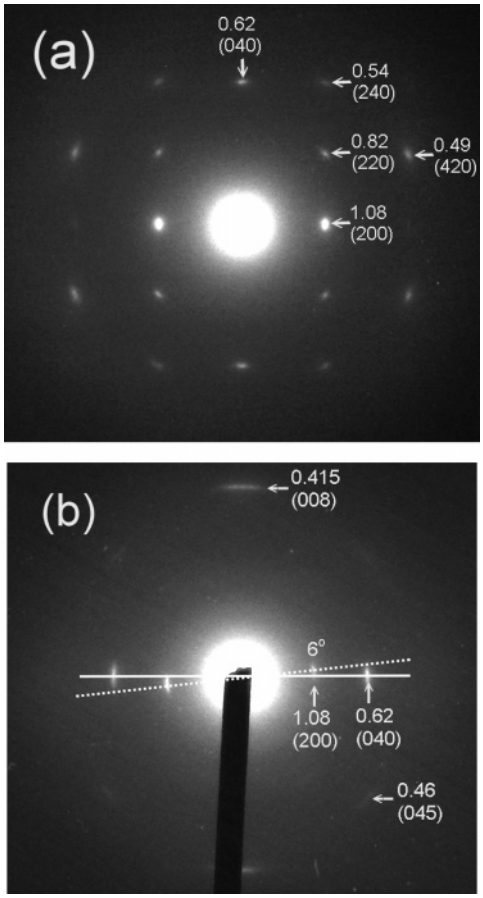

Figure 5. Expanded and indexed SAED (a) [00*l*] zone and (b) "fiberlike" patterns of the α phase for specimens (a) quickly heated to 280 °C and then crystallized at 230 °C for 15 h or (b) manually sheared at 280 °C and then crystallized at 225 °C for 1 h before final quenching in ice−water.

first proposed by Smith[24] and later advocated by Wunderlich and co-workers.[25,26] Possible space groups for the α phase include *C*2, *Cm*, or *C*2/*m*.

In comparison, SAED patterns in Figure 6 cannot be indexed in terms of a single-crystal structure but require the coexistence of two crystalline lattices of the shared *c*-axis. In addition to reflections from the α form, there exist additional reflections that are consistent with a triclinic unit cell (α′ form) with $a =$ 2.05 nm, $b =$ 2.58 nm, $c =$ 3.30 nm, and $\alpha = \beta = 96°$. The presence of reflections with odd $h + k$ values in Figure 6a signifies breaking of the 2-fold screw symmetry along the *a*-axis or a *b*-glide plane perpendicular to the *a*-axis whereas the off-axis reflections in Figure 6b indicate increased order along the backbone axis; this leads to the assignment of low symmetry space group *P*1. More detailed analysis of these SAED and XRD patterns are still in progress; results will be reported at a future time. Our main point here is the presence of two crystalline forms that essentially share the same backbone axis; the main difference is the loss of translational order along the chain axis in the α phase, which results in higher symmetry and a decreased number of spots in the corresponding SAED patterns.

Thermal Behavior. With the presence of two crystalline forms identified, we are in a better position to interpret the perplexing thermal behavior observed through DSC analysis. We begin with the cases for fixed heating/cooling rates of 20 °C/min. In the first DSC heating scan (the top curve in Figure 7a) of the as-received sample, there exists a certain exothermal reorganization below 150 °C, followed by an endothermic event near 180 °C, and a clear final melting around 250 °C. On the basis of XRD observations presented in Figure 1, we attribute the sequence of thermal events to the transformation of β mesomorph to (presumably thin) α crystals that subsequently undergo a continuous melting, reorganization, and remelting process with increasing temperature. Note that the heating traces did not return to the corresponding baseline between the two main events of β-to-α and α-to-N transitions. Upon cooling (top curve in Figure 7b), formation of α crystals commences at T_c = ca. 210 °C; the α-to-α′ transformation (expected to occur below 190 °C as demonstrated in Figure 1) does not exhibit a distinguishable second thermal event: this is attributed to the sluggish manner of the transformation process. In the reheating trace (middle curve in Figure 7a), discernible thermal events include minor reorganization above 110 °C, a broad endotherm between 180 and 220 °C (which corresponds to the α′-to-α transformation, cf. Figure 1c), a shoulder in the vicinity of 240 °C (implying melting−reorganization of α crystals), and the final melting of thickened α crystals into the nematic liquid above 250 °C. DSC traces of subsequent cooling or heating scans (cf. remaining curves in Figure 7a,b) do not show further changes. For the glassy specimen quenched from the nematic melt, the first heating trace (top curve in Figure 7c) shows the presence of glass transition (T_g) at ca. 103 °C, a sharp exotherm of cold crystallization (into α form) around 140 °C, a low-melting endotherm around 200 °C (premelting of cold-crystallized thin crystals), and without returning to the baseline (hinting continuous melting−reorganization), the final melting above 250 °C. Subsequent cooling (not shown) or reheating (bottom curve in Figure 7c) traces are essentially the same as those given in Figure 7a,b.

In the discussion above, we have tentatively neglected the difference in the mode of temperature changes in the XRD

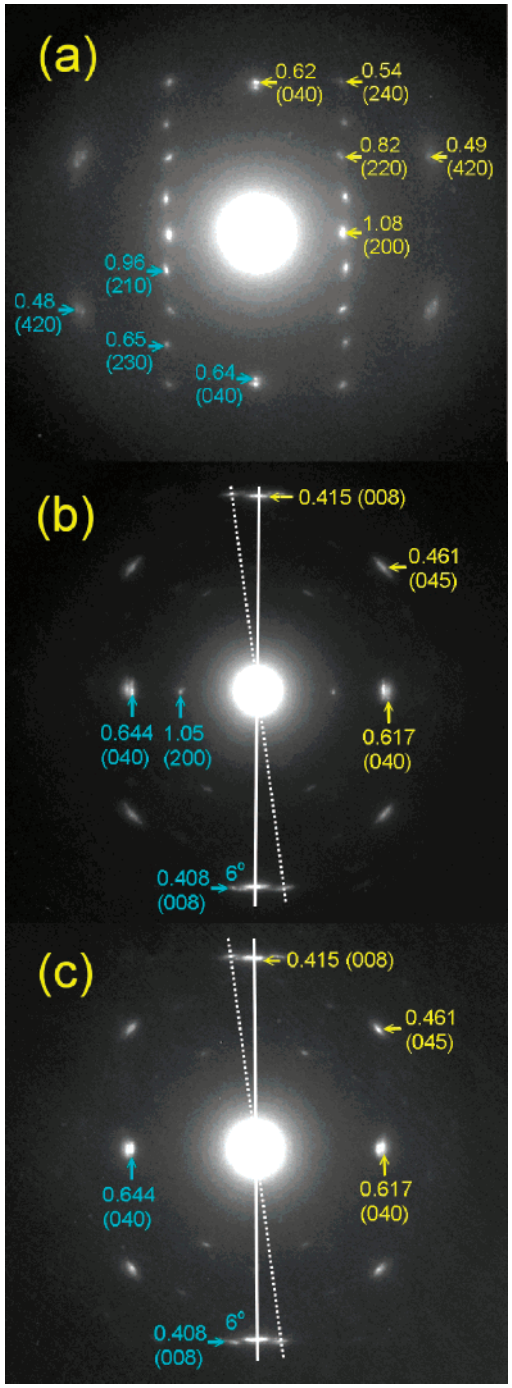

Figure 6. Expanded and indexed SAED (a) [00*l*] zone and (b, c) "fiber" patterns of coexisting α (yellow indices) and α′ (blue indices) phases. Specimens were (a) quickly heated to 280 °C and subsequently crystallized at 230 °C for 15 h followed by programmed cooling at 20 °C/min to room temperature or (b, c) manually sheared at 280 °C, followed by crystallization at 170 °C for 10 min before cooling at 20 °C/min to room temperature. In the latter cases, the shear direction is along the meridian. All patterns show approximately shared unit cell axes, with minor deviations in the vicinity of 6°. The absence of $(200)_{\alpha'}$ spots in panel c and the small size of this reflection in panel b imply preferred orientation of the *a*-axis along the film normal and slight but significant nonorthogonality.

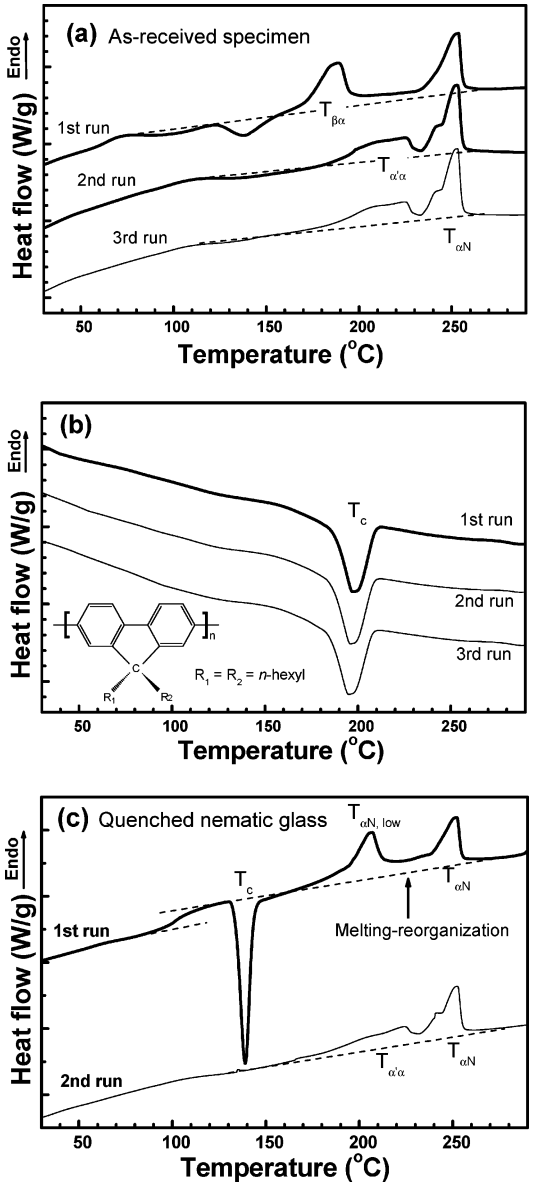

Figure 7. (a) DSC heating and (b) cooling traces of as-received PFH upon thermal cycling between ambient and 300 °C at a fixed heating/cooling rate of 20 °C/min. (c) DSC heating traces of initially nematic PFH (vitrified via quenching from 300 °C to the liquid nitrogen temperature) during thermal cycling between ambient and 300 °C. Peak assignments are made via comparison with high-temperature XRD profiles given in Figure 1.

(stepwise jumps) and the DSC (dynamic scanning) studies. In this respect, examining DSC traces at different heating or cooling rates may lend some measure of the possible effects. For the as-received sample, the first heating at a higher rate of 40 °C/min (top curve in Figure 8a) is very similar to its counterpart at 20 °C/min, with mainly two endothermic events of β-to-α and α-to-N transitions occurring in the vicinity of 185 and 250 °C, respectively. However, cooling at 40 °C/min is clearly too fast for complete crystallization (top two curves in Figure 8b). This results in a small but distinctly identifiable recrystallization peak near 140 °C upon reheating (second and third traces from the top of Figure 8a), which is delayed to a slightly higher temperature in the case of a higher heating rate of 40 °C/min. Comparison of other heating/cooling traces in Figure 8 indicates that cooling rates below 20 °C/min are adequate for the crystallization process during cooling to reach near completion.

Irrespective of the heating rate adopted, general features of reheating traces in Figure 8a are consistent with recrystallization/reorganization above T_g, α′-to-α transformation from 140 to 230 °C, followed by perfection and final melting of the α phase near 240 and 250 °C, respectively. The latter assignments are consistent with the increase in peak temperature of the final

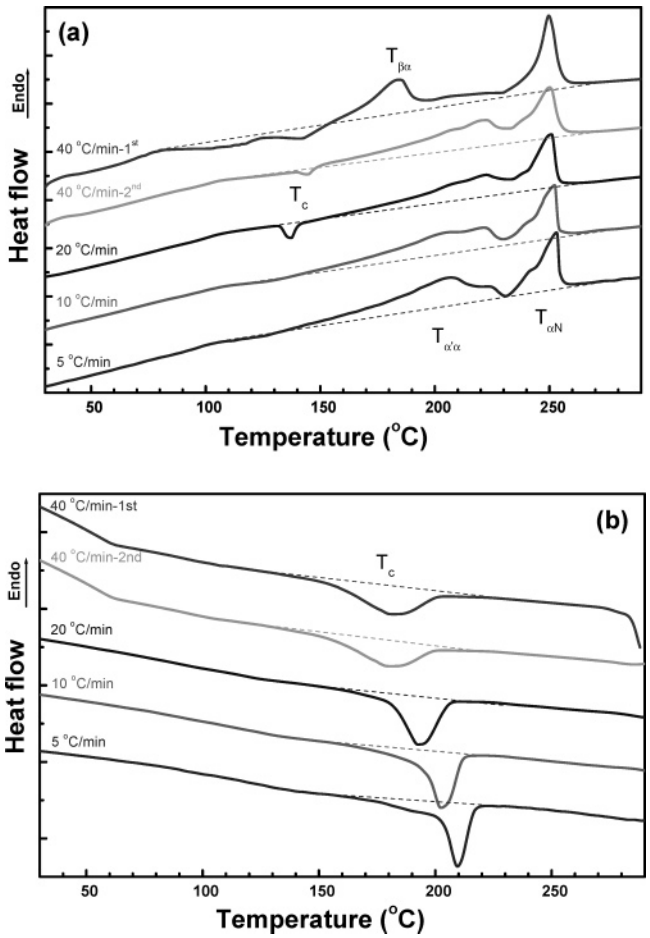

Figure 8. (a) DSC heating and (b) cooling traces of as-received PFH upon thermal cycling between ambient and 300 °C at different rates: twice at 40 °C/min first, followed by once at 20, 10, and then 5 °C/min.

melting endotherm from 250 to 253 °C as the heating rate decreased from 40 to 5 °C/min. As for cooling traces (Figure 8b), the onset and the peak temperatures of crystallization and the extent of crystallinity development depend on the cooling rate, as is commonly observed in typical semicrystalline polymers. From these cooling traces, one may deduce that the extrapolated onset temperature of crystallization (the first deviation from the baseline) upon infinitely slow cooling corresponds to ca. 240 °C, consistent with the XRD observations in Figure 1.

Thermal- and Transformation-Induced Cracking. Additional support to our assignment of two crystalline forms may be found in morphological features of PFH crystals. White stripes (enhanced by Pt-shadowing) running parallel to either *a*- or *b*-axes are easily identifiable for specimens of coexisting α and α′ crystals (Figure 3b). Corresponding SEI (cf. Figure 9) of the same specimen indicate that these correspond to *tensile* cracks running parallel to the *a*-axis and *compressive* cracks along the *b*-axis. It is very likely that these cracks are related to stresses induced by the α-to-α′ transformation during programmed cooling: the α′ unit cell is significantly shorter in the *a*-dimension (2.05 vs 2.15 nm) and longer in the *b*-dimension (2.58 vs 2.47 nm) as compared to the α form, ensuring development of compressive stresses in the *b*-direction and tensile stresses in the *a*-direction in α′ crystals upon transformation from the α phase. From XRD profiles shown in Figure 1b, we deduce that values of the linear thermal expansion coefficient for α crystals are ca. 340 ppm/K along the *a*-axis and 180 ppm/K along the *b*-axis whereas corresponding values of the α′ form are 110 and 420 ppm/K, respectively. Compared to the much lower thermal expansion of glass substrate (in the order of 10 ppm/K), both types of cracks would be opened up upon further cooling to room temperature as indeed is observed in Figure 9. The presence of transformation-induced stresses would also explain the autoinhibition or self-retardation characteristics of the α-to-α′ transformation. Despite our extensive attempts using a wide variety of thermal histories, the transformation never reaches complete conversion. It may be easily envisioned that stresses induced by partial transformation of α-to-α′ forms may prohibit further progress of the transformation process.

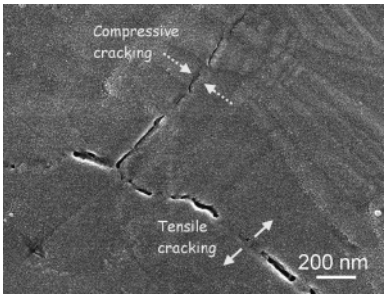

Figure 9. Representative SEI taken from the same PFH specimen (crystallized at 230 °C for 15 h, followed by programmed cooling at 20 °C/min to room temperature) presented in Figure 3b. Note the development of tensile and compressive cracks running parallel to *a*- and *b*-axes, respectively. The higher growth rate of PFH crystalline lamellae in the *b*-direction results in slender crystals running NW-SE in the upper right region, which serve to indicate crystallographic orientations; the *c*-axis of these crystals lies along the film normal, as indicated by the SAED pattern in Figure 3b. The tensile cracks are characterized by connecting fibrils. Both types of cracks were further opened up by subsequent development of thermal stresses (tensile in nature due to the much lower low thermal expansion coefficient of the glass substrate) upon cooling to room temperature.

Summarizing Remarks

Phase Behavior. All the observations above may now be summarized as the following. (1) Above ca. 253 °C, PFH exists as a nematic liquid. (2) There are two crystalline polymorphs in the solid state: the α form is the preferred high-temperature phase whereas the α′ form is thermodynamically more stable at lower temperature. Solid−solid transformation occurs reversibly (but incompletely) between the two polymorphs upon temperature changes around 190 °C. (3) The β mesomorph in the as-cast film is intrinsically metastable, which (bypassing the α′ phase) transforms directly to the α phase upon heating above 175 °C.

The observation that the triclinic α′ form is thermodynamically favored at lower temperatures whereas the monoclinic α form is more stable at temperatures above ca. 200 °C is in agreement with the general rule that the high-temperature phase is usually of higher crystal symmetry. Kinetic effects, however, are apparent. Despite extensive efforts in adopting a broad range of thermal histories, our experimental observations indicated that the formation of α′ crystals is limited to the pathway of α−α′ transformation, i.e., the α crystals always form first and serve as precursors of α′ crystals. With increasing temperatures, the transformation of the metastable β phase in the as-cast film is observed to result in α crystals only. Upon cooling from the nematic state, α crystals always form first even for large supercoolings where the α′ form is thermodynamically more stable. The energy barrier for the nucleation of α′ crystals is therefore expected to be high except for the case of transformation from α to α′ forms, which involves mainly adjustment of

backbone position along the *c*-axis, as indicated by the (approximately) shared [00*l*] zone axis in Figure 6.

Comparison with PFO. As one would expect, there exist qualitative similarities in phase behavior for the closely related pair of PFH and PFO. These include (1) the existence as a nematic liquid at high temperatures, (2) the presence of two crystalline (α and α′) polymorphs in the solid state, and (3) the intrinsic metastability of the lamellar (β) mesomorph in the as-cast films. The existence of nematic nature is certainly attributable to the rigidity of the PF backbone. The presence of structurally similar polymorphs, generally categorized as pseudo-orthorhombic with slight deviations from strict orthogonality, may now be attributed to minor translational adjustments of PF backbones along the *c*-axis for more ordered packing in the low-temperature (α′) phase. Features of intrinsic metastability of the β phase and the direct β-to-α transformation (bypassing the low-temperature α′ phase) are also shared by the two homologues. However, there exists a qualitative difference. The origin of the β phase here is different from its counterpart in the case of PFO, which is a degenerate form of a crystalline clathrate phase that appears first in the early stage of film formation and is easily dissipated around 100 °C (cf. Figure 2 in ref 22). In the present case of PFH, such a major crystalline precursor cannot be identified (cf. Figure 2a) and some residual β phase may persist up to a much higher temperature of ca. 250 °C (cf. Figure 1a).

Acknowledgment. Financial support from the Ministry of Education (grant no. 91-E-FA04-2-4A) and the National Science Council (grant no. NSC93-2216-E-110-001) is gratefully acknowledged.

References and Notes

(1) Kraft, A.; Grimsdale, A. C.; Holmes, A. B. *Angew. Chem., Int. Ed.* **1998**, *37*, 402.
(2) Neher, D. *Macromol. Rapid Commun.* **2001**, *22*, 1365.
(3) Scherf, U.; List, E. J. W. *Adv. Mater.* **2002**, *14*, 477.
(4) Grell, M.; Bradley, D. D. C.; Inbasekaran, M.; Woo, E. P. *Adv. Mater.* **1997**, *9*, 798.
(5) Teetsov, J.; Fox, M. A. *J. Mater. Chem.* **1999**, *9*, 2117.
(6) Blondin, P.; Bouchard, J.; Beaupre, S.; Belletete, M.; Durocher, G.; Leclerc, M. *Macromolecules* **2000**, *33*, 5874.
(7) Kawana, S.; Durrell, M.; Lu, J.; Macdonald, J. E.; Grell, M.; Bradley, D. D. C.; Jukes, P. C.; Jones, R. A. L.; Bennett, S. L. *Polymer* **2002**, *43*, 1907.
(8) Grell, M.; Bradley, D. D. C.; Long; X.; Chamberlain, T.; Inbasekaran, M.; Woo, E. P.; Soliman, M. *Acta Polym.* **1998**, *49*, 439.
(9) Grell, M.; Bradley, D. D. C.; Ungar, G.; Hill, J.; Whitehead, K. S. *Macromolecules* **1999**, *32*, 5810.
(10) Redecker, M.; Bradley, D. D. C.; Inbasekaran, M.; Woo, E. P. *Appl. Phys. Lett.* **1999**, *74*, 1400.
(11) Lee, J. I.; Klaerner, G.; Miller, R. D. *Synth. Met.* **1999**, *101*, 126.
(12) Ariu, M.; Lidzey, D. G.; Bradley, D. D. C. *Synth. Met.* **2000**, *111*−*112*, 607.
(13) Herz, L. M.; Phillips, R. T. *Phys. Rev. B* **2000**, *61*, 13691.
(14) Cadby, A. J.; Lane, P. A.; Mellor, H.; Martin, S. J.; Grell, M.; Giebeler, C.; Bradley, D. D. C.; Wohlgenannt, M.; An, C.; Vardeny, Z. V. *Phys. Rev. B* **2000**, *62*, 15604.
(15) Ariu, M.; Lidzey, D. G.; Lavrentiev, M.; Bradley, D. D. C.; Jandke, M.; Strohriegl, P. *Synth. Met.* **2001**, *116*, 217.
(16) Ariu, M.; Lidzey, D. G.; Sims, M.; Cadby, A. J.; Lane, P. A.; Bradley, D. D. C. *J. Phys.*: *Condens. Matter* **2002**, *14*, 9975.
(17) Korovyanko, O. J.; Vardeney, Z. V. *Chem. Phys. Lett.* **2002**, *356*, 361.
(18) Winokur, M. J.; Slinker, J.; Huber, D. L. *Phys. Rev. B* **2003**, *67*, 184106.
(19) Khan, A. L. T.; Banach, M. J.; Köhler A. *Synth. Met.* **2003**, *139*, 905.
(20) Chen, S. H.; Chou, H. L.; Su, A. C.; Chen, S. A. *Macromolecules* **2004**, *37*, 6833.
(21) Chen, S. H.; Su, A. C.; Su, C. H.; Chen, S. A. *Macromolecules* **2005**, *38*, 379.
(22) Chen, S. H.; Su, A. C.; Chen, S. A. *J. Phys. Chem. B* **2005**, *109*, 10067.
(23) Chen, S. H.; Su, A. C.; Chang, C. S.; Chen, H. L.; Ho, D. L.; Tsao, C. S.; Peng, K. Y.; Chen, S. A. *Langmuir* **2004**, *20*, 8909.
(24) Smith, G. W. In *Advances in Liquid Crystals*; Brown, G. H., Ed.; Academic Press: New York, 1975; Vol. 1, p 193.
(25) Wunderlich, J.; Grebowicz, B. *Adv. Polym. Sci.* **1984**, *60*/*61*, 1 and references therein.
(26) Wunderlich, J. *Thermochim. Acta* **1999**, *340*/*341*, 37 and references therein.